

L-Arginine Binding to Human Inducible Nitric Oxide Synthase: An Antisymmetric Funnel Route toward Isoform-Specific Inhibitors?

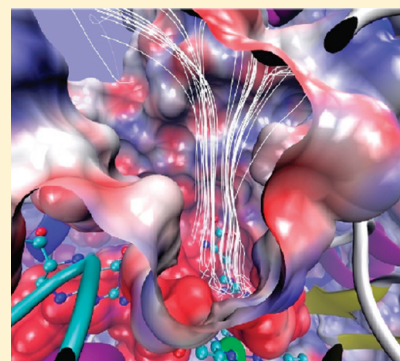
Nicolas Floquet,^{*†} Jean-François Hernandez,[†] Jean-Luc Boucher,[‡] and Jean Martinez[†]

[†]Institut des Biomolécules Max Mousseron (IBMM), UMR 5247 Université Montpellier 1, Université Montpellier 2, CNRS, Faculté de Pharmacie, 15 Avenue Charles Flahault, B.P. 14491, 34093 Montpellier Cedex 05, France

[‡]Laboratoire de Chimie et Biochimie Pharmacologiques et Toxicologiques, CNRS UMR8601, Université Paris Descartes, 45 Rue des Saints-Pères, 75270 Paris, France

 Supporting Information

ABSTRACT: Nitric oxide (NO) is an important signaling molecule produced by a family of enzymes called nitric oxide synthases (NOS). Because NO is involved in various pathological conditions, the development of potent and isoform-selective NOS inhibitors is an important challenge. In the present study, the dimer of oxygenase domain of human iNOS (iNOSOxy) complexed to its natural substrate L-arginine (L-Arg) and both heme and tetrahydro-L-biopterin (BH4) cofactors was studied through multiple molecular dynamics simulations. Starting from the X-ray structure available for that complex (PDB: 1NSI), a 16 ns equilibration trajectory was first obtained. Twelve dynamics of slow extraction of L-Arg out from the iNOSOxy active site were then performed. The steered molecular dynamics (SMD) approach was used starting from three different points of the reference trajectory for a total simulation time of 35 ns. A probable unbinding/binding pathway of L-Arg was characterized. It was suggested that a driving force directed the substrate toward the heme pocket. Key intermediate steps/residues along the access route to the active site were identified along this “funnel shape” pathway and compared to existing data. A quasi-normal mode analysis performed on the SMD data suggested that large collective motions of the protein may be involved in L-Arg binding and that opening the route to the active site in one monomer promoted an inverse, closing motion in the second monomer. Finally, our findings might help to rationalize the design of human iNOS isoform competitive inhibitors.



INTRODUCTION

Nitric oxide (NO) produced by mammalian nitric oxide synthases (NOSs) acts as a second messenger in the cardiovascular and nervous systems and as a cytotoxic agent in the immune system.¹ Three NOS isoforms (neuronal, endothelial, and inducible, nNOS, eNOS, and iNOS, respectively) produce NO by oxidation of the L-Arg substrate.^{1,2} Constitutive nNOS and eNOS are calcium dependent and generate low levels of NO for short periods, whereas iNOS expression is induced by pro-inflammatory cytokines, is calcium-independent, and produces high levels of NO for longer times.³

All three NOS isoforms share a common multidomain organization comprising an N-terminal oxygenase domain (NOSOxy), an intercalated calmodulin binding domain and a C-terminal reductase domain. They are functional only as homodimers, dimerization ensured by the oxygenase domain being required for proper activity.^{4–6} Many X-ray structures of all three isoforms have been solved covering different species. Most of these structures describe the NOSOxy domains complexed to a large panel of L-Arg and analogues. However, no structure of the full-length enzyme is yet available. The catalytic active site of NOSs is provided by the NOSOxy domain that binds the heme prosthetic group and the redox cofactor tetrahydrobiopterin (BH4). The

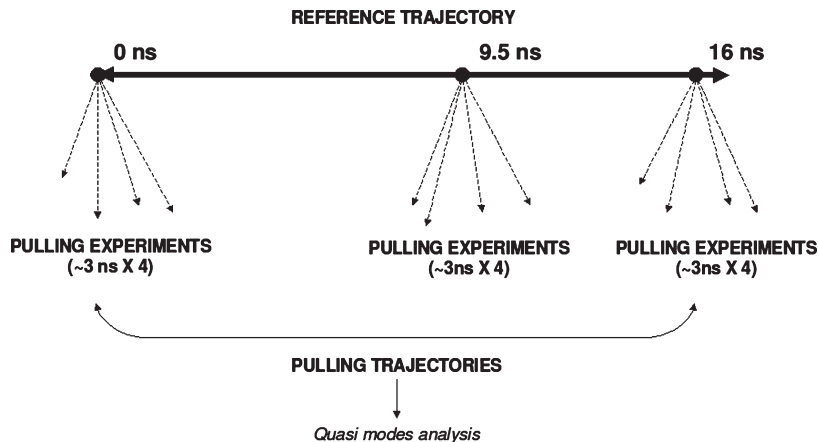
NOS reductase domain has NADPH as cofactor and binding sites for flavins FAD and FMN.^{4–6}

Overproduction of NO by nNOS or iNOS is associated with various pathological disorders. Inducible NOS contributes to a large panel of pathologies possessing an inflammatory component, including septic shock,⁷ arthritis,⁸ neurodegenerative disorders,^{9–11} obesity/diabetes,^{12,13} and cancers^{14,15} and thus constitutes an important pharmacological target. Inhibition of iNOS has numerous potential applications, but the identification of potent, highly iNOS selective, non toxic, and bioavailable inhibitors remains an important pharmacological challenge, and no molecule has been yet put on the market.¹⁶

Crystal structures of the oxygenase domains of the three mammalian NOSs have identified key amino acid residues involved in the binding of L-Arg substrate and BH4 cofactor. They showed that the α -amino function of L-Arg is a key factor for binding at the NOSs active sites and that a highly conserved crucial Glu residue (Glu377 in human iNOS) forms a salt bridge with the guanidine moiety of L-Arg and also hydrogen (H)-bonds with its α -NH₂ group.^{17–20} Furthermore, these crystallographic

Received: October 25, 2010

Published: May 16, 2011

Scheme 1. Summary of the Protocol Used during This Study

studies revealed a H-bond network involving L-Arg, diatomic ligands, and active-site water molecules that could be involved in proton shuttling during catalysis.^{21,22} These studies have shown a striking degree of conservation of the L-Arg binding site among all three isoforms explaining the encountered difficulties to design isoform-selective L-Arg competitive inhibitors. Nevertheless, some significant differences were revealed, especially in the putative substrate access channel to the active site.²³ These observations have increased the interest in the design of large molecules as inhibitors extending out from the active site toward this access channel. Robert B. Silverman mainly developed this approach for the inhibition of nNOS by substrate-based dipeptides.²⁴ The recent work of Garcin et al. demonstrated a plasticity of this channel in murine iNOS that allows specific interactions with second-shell nonconserved residues.²⁵ The binding mode of these selective inhibitors could be defined only by X-ray crystallographic studies and would have been hardly predicted by molecular modeling using existing crystal structures.

X-ray structures constitute the necessary material to start with molecular mechanics studies. However, they trap only static conformational states without any information on intermediates that may also be biologically relevant. There is an interest to identify residues and/or segments of importance inside the active sites of NOSs and/or in their substrate access channels to better understand and predict the binding modes of new ligands. New molecular dynamics data not (or poorly) obtained by crystallographic studies should help to design and synthesize new potent inhibitors with high selectivity for one NOS isoform. We hypothesized that studying substrate binding to NOSs by molecular modeling might provide some of these informations. Binding L-Arg is an essential event in NO synthesis and understanding the NOSs–substrate interactions in more detail is important for developing highly selective inhibitors.

We have used computational methods to study the possible dynamical mechanism of L-Arg binding to the human iNOSOxy active site at the molecular level. Such a mechanism may not be observed during nanosecond time scale molecular dynamics simulations, and we employed the steered molecular dynamics (SMD) approach which allows to fit biologically relevant phenomena to computationally compatible simulation times.²⁶ In some recent representative examples, the SMD approach was used to pull D-Glu out from the glutamate racemase enzyme,²⁷ to study phenol escape dynamics out from insulin,²⁸ or to study

ligand unbinding mechanism in estrogen receptors.²⁹ SMD was used here to slowly pull L-Arg out from the active site of human iNOSOxy. In all this study, we hypothesized that the most favorable unbinding pathway(s) for L-Arg may be identical to the binding one(s). This starting hypothesis permitted us to start with a known crystallographic position of L-Arg in the iNOSOxy active site [Protein Data Bank (PDB) structure: 1NSI].¹⁹ We showed that the unbinding/binding of L-Arg to iNOSOxy followed a “funnel shape” route with key residues along this route. From our calculations, we further proposed that the binding of L-Arg might occur in one monomer, then in the second. Finally, we showed that structures generated along the obtained pulling trajectories can already improve the results of docking experiments performed against the human enzyme.

MATERIAL AND METHODS

Initial Structure. The molecular modeling of the dimer of the oxygenase domain of human iNOS was performed using the available X-ray data deposited in the PDB: 1NSI,¹⁹ resolution 2.55 Å.

BH4 cofactor parameters were derived for the CHARMM force field using Gaff, Antechamber, and Charmmgen programs.^{30,31} Heme parameters were those described in the CHARMM parameters files.³² Molecular modeling of cysteines bridged either to the Zn²⁺ ion at the dimer interface or to the iron atom of the heme was performed using the CYM or CYC residues, respectively, which parameters have also been previously described in the CHARMM forces field.^{33,34}

Protocol. The employed protocol is summarized in Scheme 1.

Molecular Dynamics Simulations. Molecular dynamics simulations were performed in a TIP3 water box assuming at least 10 Å of water on each side of the protein. The NAMD software³⁵ was used together with the CHARMM force field parameters set 22.³² The Verlet algorithm was used with a 1 fs integration step, and nonbond interactions were treated using a cutoff of 12.0 Å (switching function applied between 10.0 and 12.0 Å). An unconstrained 16 ns trajectory was obtained as a first step.

Extraction of L-Arg was performed using the steered molecular dynamics approach as implemented in NAMD. In brief, the SMD approach consisted of biasing the simulation behavior along a particular reaction coordinate and allowing the study of biologically relevant processes during simulations on the nanosecond

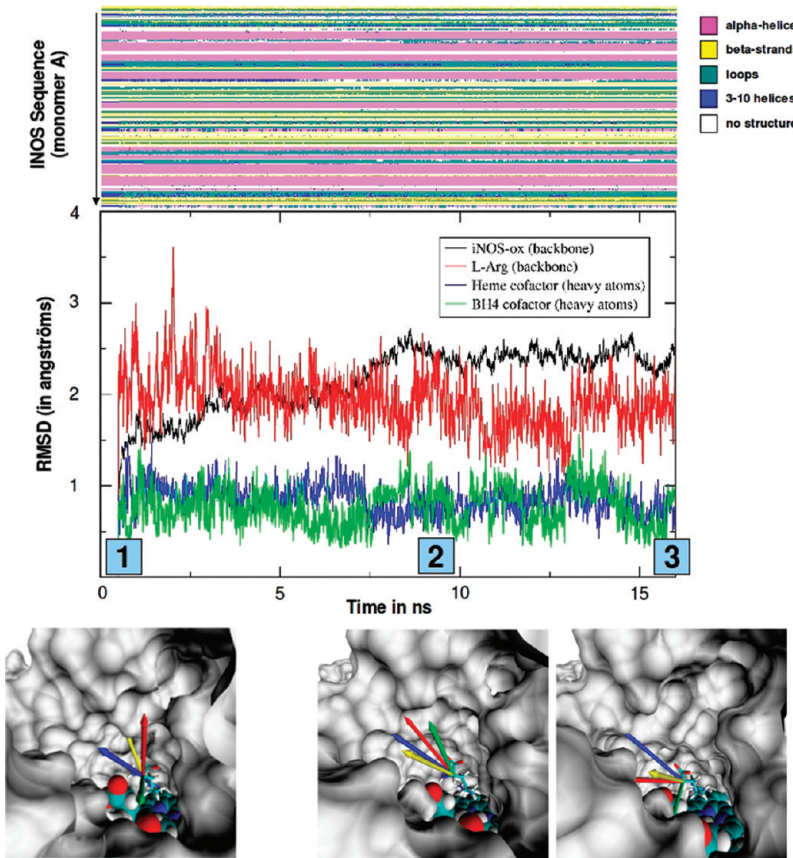


Figure 1. RMSD versus time evolution for different parts of the system and along the unconstrained molecular dynamics trajectory. A stable conformation was reached after 10 ns of dynamics. The graph in the top showed the stability of the secondary structure elements (pink: α -helix; yellow: β -strands) of the enzyme during that stage. In the following, three different configurations of the system were retained: points 1 (0 ns), 2 (9.5 ns), and 3 (16 ns) to perform pulling experiments of the L-Arg ligand. Four pulling directions were randomly chosen for each of these points, as graphed in the bottom of the figure.

time scale. Three different points of the initial unconstrained trajectory were selected for constant velocity pulling experiments at respectively 0, 9.5, and 16 ns. $C\alpha$ of L-Arg was chosen as the pulled atom. For each of the three starting configurations, four different pulling directions were followed, with a spring constant of $50 \text{ kcal} \cdot \text{mol} \cdot \text{\AA}^2$ and a very slow constant velocity of $0.000005 \text{ \AA} \cdot \text{fs}^{-1}$ (e.g., $5 \text{ \AA} \cdot \text{ns}^{-1}$). This velocity was of the same order than those used in other recent studies.^{27–29}

Quasinormal Modes Analysis (“Essential Dynamics”). Quasimodes reflect the large, collective, motions of the protein described in a molecular dynamics trajectory. Quasimodes analysis was performed on all concatenated SMD trajectories using CHARRMM and all the snapshots of the trajectories, which were registered every 1 ps.

Docking Experiments. Docking experiments were performed with the VINA software³⁶ in a region of 20 \AA around the iron atom of the heme bound cofactor. Ligands were extracted from their respective X-ray structures after a structural fit was performed on the 1NSI structure. Structures of the ligands were then converted to the PDBQT format using autodocktools scripts.^{37,38} Structures of iNOS were converted to the PDBQT format. Representative conformations of the active site and the access route of human iNOS were selected from the SMD molecular dynamics trajectories. Clustering of the sampled conformations was performed as previously explained,³⁹ using the residues of the region of interest to compute 2D root-mean-square deviation

(RMSD) matrices prior to performing a hierarchical clustering. Hydrogen atoms were added to both ligand and protein structures using Openbabel. BH4 and heme cofactors were also included in the calculations, whereas all water molecules were removed. During the docking experiments, the target was kept rigid, whereas the flexibility of the ligands was explored in the full dihedral space.

RESULTS

Building of the Initial Model. The starting structure used for the calculations and describing the human iNOSOxy complexed to L-Arg (PDB: 1NSI)¹⁹ was subjected to a first molecular dynamics simulation in explicit solvent without applying any constraint. Tetrahydro-L-biopterin parameters were defined using Gaff and antechamber.^{30,31} RMSDs were computed for the protein, the substrate L-Arg, and the cofactors along this trajectory and are reported in Figure 1. For clarity, the RMSDs of L-Arg, heme and BH4 are reported solely for monomer A, but closely related results were obtained for the second monomer B. These RMSDs variations indicated no significant conformational change, especially for L-Arg and heme or BH4, therefore validating the semiautomated design of BH4 parameters. Theoretical B-factors were also computed for each $C\alpha$ and compared to those stored in the initial PDB: 1NSI file. Overall, the computed and the theoretical values were quite nicely correlated (see Figure S1,

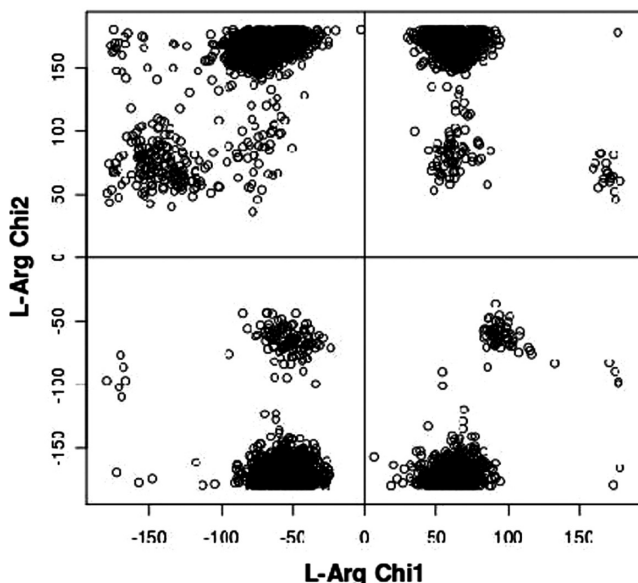


Figure 2. Chi1:chi2 plot of L-Arg along all the computed SMD trajectories showing that the chosen pulling velocity permitted conformational changes of the ligand.

Supporting Information). Computing the secondary structures in monomer A versus time also did not reveal any significant structural rearrangement (Figure 1).

Unbinding Simulations of L-Arg out from the Human iNOSOxy Active Site. Three different configurations of the system were selected from the initial trajectory [points 1 (0 ns), 2 (9.5 ns), and 3 (16 ns)] as reported by the blue boxes in Figure 1 and subjected to SMD. In that case, the SMD approach consisted of inducing L-Arg unbinding from its active site during molecular dynamics simulations in the nanosecond time scale. Such a process of unbinding might not be observed during unconstrained classical molecular dynamics simulations or might appear in the micro- to millisecond time scale that constitute unreachable times of simulations. A small force was applied to L-Arg through a low constant velocity of $0.000005 \text{ \AA} \cdot \text{fs}^{-1}$ (e.g., $5 \text{ \AA} \cdot \text{ns}^{-1}$), pulling L-Arg in four different directions for each selected starting configuration. Using these parameters, each of the 12 pulling trajectories ended in the range of 3–5 ns. In each independent simulation, this time was sufficient to bring L-Arg out from the enzyme structure. Importantly, the pulled L-Arg was also able to change conformation during the trajectories, as shown by the plot of chi1:chi2 of L-Arg in Figure 2. This demonstrated that the chosen velocity was sufficiently low to allow local rearrangements of both ligand and protein. In our simulations, unbinding of L-Arg was performed only in one monomer of iNOSOxy. Nevertheless, it was noted that in the second monomer, the second molecule of L-Arg did not encounter any significant reorientation as compared to its starting position in the crystal structure.

The energy of interaction of L-Arg with the complete system (including heme and BH4 but excluding water molecules) was computed along each of the 12 pulling trajectories. The resulting plots were reported in Figure 3a. The connection between these interactions and the successive positions of the C α of L-Arg during all the pulling experiments was reported in Figure 3b. It can be noted here that the related points expressed the requirement of conformational changes upon ligand unbinding/binding, especially in the environment of the mouth of the channel

around Ala282. This combined analysis presented in Figure 3a and b demonstrated that the interactions of L-Arg with the complete system became less important, as it was far from its starting point. This was observed for each pulling trajectory and for each starting configuration (points 1–3) and strongly suggested the existence of a driving force guiding the substrate toward the heme pocket once it has entered the access channel of iNOSOxy. Importantly, it was observed that the loss of interaction energy between the ligand and the protein was not fully compensated by the increased solvation of the ligand. The understanding of this “driving force” might of course find applications in the design of inhibitors.

Unfortunately, the pulling forces applied to L-Arg and registered for each obtained trajectory were not significantly different enough to identify a preferred exit pathway. Thus, the 12 obtained pulling trajectories were concatenated to perform a statistical analysis (see Material and Methods Section) of L-Arg positions along all the sampled pathways. The statistically most explored unbinding pathway was reported (Figure 4, pink surface).

This pathway was almost linear from the active site to the bulk solvent and followed the longitudinal axis of helix 7a, a key-structure involved in dimerization of NOSs.^{17,40} Moreover, considering its first half, this pathway was not larger than L-Arg diameter indicating common features of extraction among all of the 12 pulling trajectories. This diameter increased progressively when getting closer to the mouth of the channel, indicating multiple possible pathways of extraction and less constant interactions as already depicted in Figure 3b. The exhaustive list of residues in close contact with the ligand (distance $<3.0 \text{ \AA}$) among the 12 pulling trajectories included: W90, S92, G93, M120, T121, A262, Q263, R266, A282, N283, V284, E285, F286, P350, V352, N354, M355, G371, W372, Y373, M374, E377, R381, Q387, R388, W463, E494, W496, and K497. Among these residues, V352, Y373, and R381 are important residues for L-Arg binding in NOSs.^{41–43} A statistical analysis equivalent to that performed for the successive positions of L-Arg permitted to reduce this set of residues to P350, G371, W372, Y373, M374, and E377 (first shell residues, green sticks/meshes in Figure 4), R266 and R388 (second shell residues, violet sticks/meshes), and A282 and W90 (third shell residues, red sticks/meshes) delimiting the most occupied unbinding pathway of L-Arg.

Key Events for L-Arg Unbinding/Binding. Among the residues in close contact with L-Arg, the side chain of Glu377 is of particular interest as it establishes strong H-bonds between its COOH-group and both the α -NH₂ group and the guanidinium moiety of L-Arg.^{17,18,20} Along most of the characterized trajectories, Glu377 side chain swung from its initial crystallographic position when L-Arg was going out from the active site. This rotation was followed by a change in the interaction of Glu377 with the BH4 cofactor, suppressing the network interactions between BH4 and one of the heme propionate. This phenomena is in agreement with the structure observed for eNOSOxy bound to 7-nitroindazole.^{44,45} We also showed that in some cases this rotation was able to promote a slight translation of helix 7a. Two representative examples of Glu377 rotation from two different trajectories are depicted in Figure 5a.

Once the ligand passed through, the side chain of Glu377 was most often going back to its starting position as observed in the X-ray structure, suggesting that the side chain of Glu377 might follow L-Arg when it binds/unbinds to iNOSOxy. Motion of the side chain of Glu377 residue has been observed in several X-ray structures of NOSs. In particular, it was observed that in the case

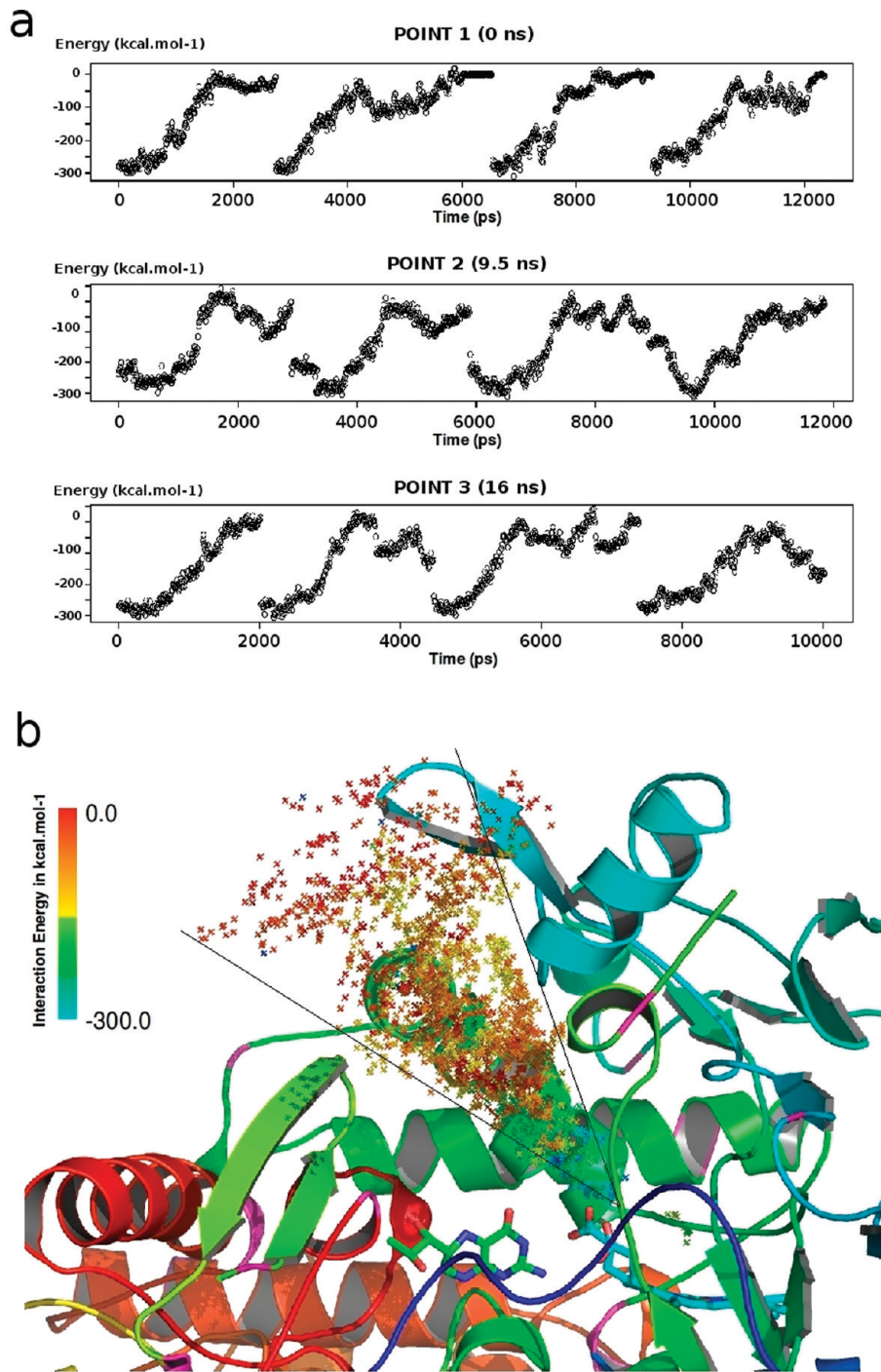


Figure 3. (a) Nonbonded energy of interaction computed between pulled L-Arg and the complete system (excluding water molecules) during the different SMD pulling trajectories performed at points 1 (0 ns), 2 (9.5 ns), and 3 (16 ns). (b) The successive positions of the C- α of L-Arg among the 12 pulling trajectories were extracted and colored according to the related energies of interaction (cold colors = stronger energies). This showed that the closer the ligand was from its crystallographic position, the higher was the corresponding interaction energy. It also showed that the farther the ligand was from this position, the wider was the “funnel shape” access to the active site.

of ligands unable to mimic the guanidinium moiety of L-Arg, the Glu377 residue was not properly oriented.^{45,46} It was also noted that the side chain of Glu377 can tilt about 10° in iNOSOxy crystallized in the presence of imidazole but in the absence of L-Arg and BH4.⁴⁷ The motion of Glu377 can also be guessed from its increased B-factor in the PDB structures describing the

unbound NOS,^{47,48} suggesting a higher flexibility than in ligand–enzyme complexes. We can here suggest that the side chain of Glu377 can effectively adopt different rotamers in the L-Arg free iNOSOxy. When the ligand comes close enough, the side chain of Glu377 might fully rotate to strongly interact with it and finally drives it to its final position in the active site.

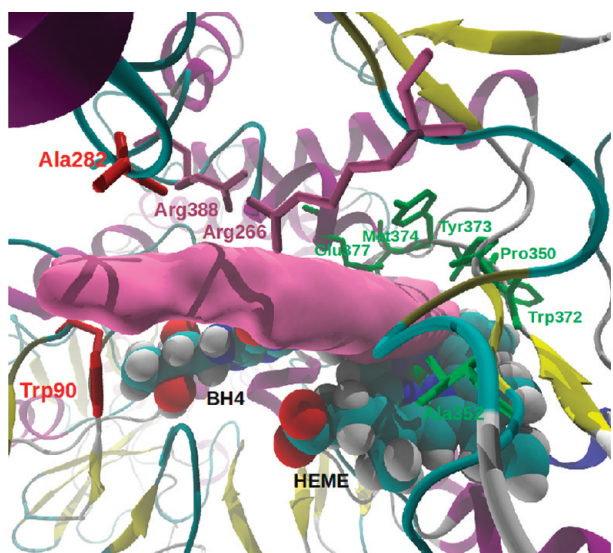


Figure 4. Visual representation of the statistical pathway of L-Arg (pink surface) among the 12 pulling trajectories. The residues which were the most in contact with the ligand are reported in green, pink, and red. The density map was computed with the Volmap tool as implemented in the VMD software.⁵⁴

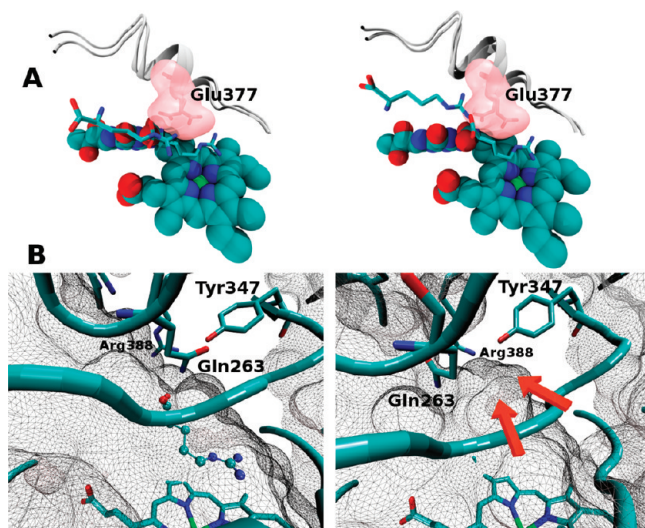


Figure 5. (A) Putative role of Glu377 in L-Arg binding. In agreement with several experimental data,^{44,45} this residue was observed to fully rotate in most of the SMD trajectories. Two examples are presented (left: point 1, red pulling direction ; right: point 2, blue pulling direction). In each case, the two extreme positions of Glu377 were reported together with the corresponding position of L-Arg. (B) Role of Gln263 flipping in the opening of an iNOSOxy specific subpocket. Our data confirmed the observations made previously by Garcin et al.²⁵

Another interesting behavior was that of residue Gln263. Garcin et al. recently demonstrated that some ligands were able to promote a rotation of this residue and therefore to open an iNOS-specific subpocket that might be important for isoform-specific ligand design.²⁵ This rotation was also observed during our molecular dynamics simulations, as shown in Figure 5b. When L-Arg was at its initial position (box on the left), Gln263 was stabilized by a H-bond with Tyr347, as previously described.²⁵

When L-Arg was pulled and getting closer to Gln263, it promoted a rotation of this residue toward Arg388, opening the so defined Gln-specific subpocket (see box on the right).

In the first events of all pulling experiments, it is also interesting to note that the α -NH₂ group of L-Arg always quickly lost its H-bond with Glu377 but conserved its interaction with one heme propionate for a longer time. In the following steps, and along most of the explored pulling pathways, the α -NH₂ of L-Arg was transiently interacting with the carbonyl group of BH4 and thereafter with water molecules that populate the access channel to the active site. The COOH-group of L-Arg initially interacted with Tyr373 and Gln263. After the breaking of these two interactions, Tyr373 and Gln263 kept together and interacted directly with each other. The COOH-group of L-Arg was then caught by the two Arg266 and Arg388 residues before being fully solvated.

Water Molecules and Channel Hydration. Importantly, we included cocrystallized water molecules in our model to finalize the solvation shell around the whole dimeric protein. In NOSs, water molecules play key roles in both the catalytic cycle and in the L-Arg binding process.^{21,22} For instance, a conserved water molecule bridges the C=O of BH4 cofactor to the residue R381; another conserved water molecule bridges the nitrogen N3 of BH4 to one of the heme propionate, also participating to L-Arg binding in the active site. During our pulling trajectories, these water molecules were always standing at their initial place. We can suggest that this might facilitate L-Arg transport by preventing a too strong interaction with the heme propionate and/or the carbonyl group of BH4 during the binding process.

Another key water molecule revealed by crystallographic studies is that lying at the top of the iron atom of the heme.²¹ This water molecule was not present in the starting model used for our calculations; nevertheless, it was present at this place just after L-Arg has left its initial bound position, thorough all the trajectories. These data are consistent with spectroscopic studies that have shown that in the absence of L-Arg, the heme-Fe^{III} was in a low-spin hexacoordinated state and in a high-spin pentacoordinate state in the presence of L-Arg.

Possible Implication of Large Collective Motions. In the SMD simulations, the process of unbinding/binding is accelerated by the force applied to the pulled atom (e.g., C α of L-Arg), so this process can be described by nanosecond time scale molecular dynamics simulations. In agreement, and even using a much smaller pulling velocity, such simulations always neglect large amplitude, collective motions of the protein; this is particularly true for proteins as big as NOSs. Nevertheless, such collective motions of NOSs might also be involved in the binding process but occur up to the millisecond time scale.^{49–51}

Because such types of motions cannot be explored by molecular dynamics simulations, their possible implication in L-Arg binding was studied through a quasinormal-mode analysis of the data obtained along the SMD trajectories. In brief, quasinormal modes or “essential dynamics” capture the collective motions through a principal component analysis (PCA) of the coordinates. Here, the included coordinates are only those of the C α of both the protein and the ligands. Among the 50 computed normal modes, we were particularly interested in the lowest frequency modes that described an uprising of the ligand in the access channel to the active site. Among all the computed modes, only one was full filling this condition, e.g., mode 9 represented in Figure 6a. Interestingly this mode described an opening of the monomer in which the ligand was pulled (monomer A). Indeed

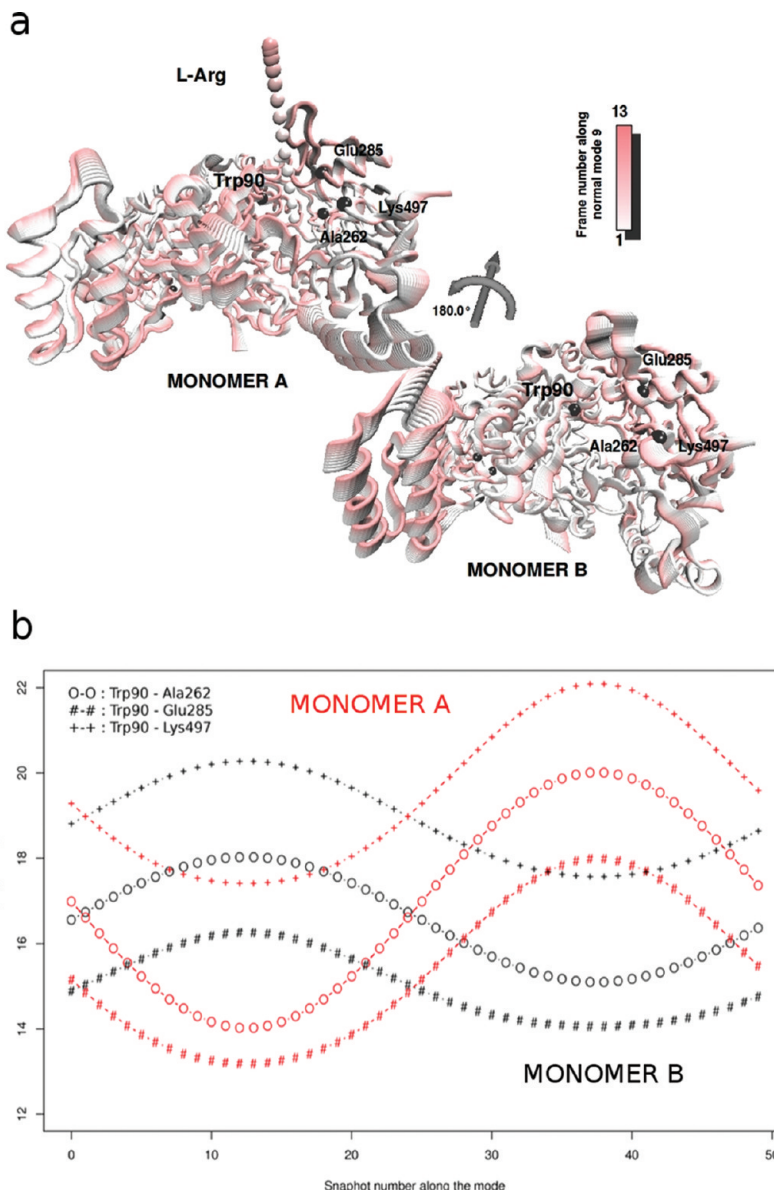


Figure 6. (a) Motions of the dimeric iNOSOxy along one of the lowest frequencies normal modes (mode 9) as extracted from the concatenated pulling trajectories (quasimodes analysis). The unbinding/binding of L-Arg in one monomer promoted an opening motion of the access channel to the active site and an inverse (closing) motion in the second monomer. (b) Three interatomic distances have been chosen to monitor the opening/closing motions in both monomers, e.g., Trp90:Ala262, Trp90:Glu285, and Trp90:Lys497.

and as already mentioned, the exit of the ligand out from the active site required some local deformations especially at the mouth of the channel. This opening was quantified in Figure 6b by the increase of the three Trp90:Ala262, Trp90:Glu285, and Trp90:Lys497 C α -C α distances. Surprisingly, it was observed that the same three distances decreased in the other monomer (monomer B) as confirmed by visual analysis of Figure 6a. In monomer B, the amplitudes of the monitored distances were significantly lower than in monomer A, probably due to the fact that only one L-Arg was pulled (monomer A), while the other was held in place in the active site (monomer B). These results suggest that the binding/unbinding of ligands in the human iNOS, and possibly by extension in NOS isoforms, might promote an opening of the access channel to the active site in one monomer and an inverse, closing motion in the second one.

This finally suggests that L-Arg binding/unbinding in NOSs may occur successively in one monomer and then in the other.

These observations deserve interest as it was suggested that the two binding sites of the NOSs might have different behaviors with cooperation between L-Arg and BH4 binding but anticopoperation between BH4 binding sites.^{52,53}

Consequences for Ligand(s)-Protein Docking Experiments. To test the possible application of our simulations on molecular docking experiments, we selected a set of 53 iNOS ligands whose three-dimensional structures of complexes with iNOSOxy were available in the PDB. These complexes described mainly murine iNOS L-Arg competitive inhibitors. After extraction, the 53 corresponding ligands were docked with VINA³⁶ onto each of the 53 corresponding X-ray structures to test the efficiency of the docking method ($53 \times 53 = 2.809$ docking

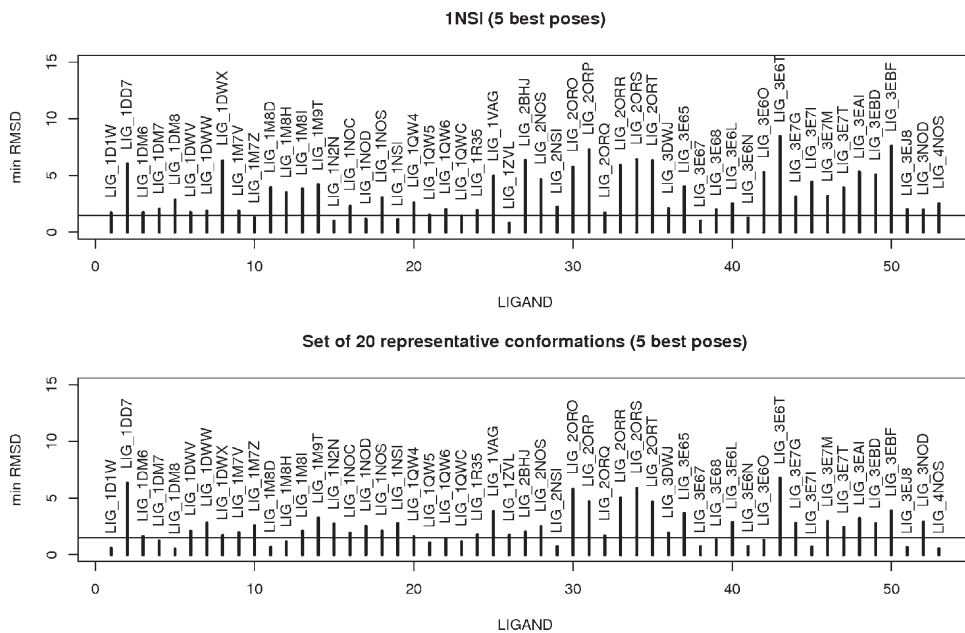


Figure 7. Docking results of 53 iNOS ligands whose positions are known in the PDB. Docking was performed in either the starting X-ray structure of human iNOS (PDB:1NSI, upper graph) or in a set of 20 representative conformations of the access channel to the active site, as extracted from the SMD pulling trajectories (bottom graph). Below the horizontal line (min RMSD = 1.5 Å) the position of the ligand was considered as correctly predicted. This showed that the use of the structures obtained along the molecular dynamics simulations significantly improved the results of docking for many ligands.

combinations). The poses were evaluated using the internal scoring function of VINA; to have a detailed description of this scoring function, please see the work of Trott and Olson.³⁶ For each ligand, the best ranked position that was found in each of the 53 conformations of the target was concatenated with the others. A ligand was considered as correctly predicted when at least one of these 53 solutions shared a RMSD < 1.5 Å with the crystallographic solution. Considering this, it was concluded that VINA was nicely able to replace 80% of these ligands.

Docking experiments were then performed with the same set of ligands but either onto the PDB: 1NSI¹⁹ structure of human iNOSOxy that was used as a starting point in this study or on a set of 20 representative conformations of the enzyme that were extracted from the SMD trajectories. Clustering of the entire set of conformations of the protein into 20 representative ones was performed as described previously³⁹ and considering the residues 120, **121**, **262**, 263, 266, 282, **283**, **284**, 286, 285, 350, 352, 354, 355, 371, 372, 373, 374, 377, 381, 389, 388, 463, 494, 496, and 497 for RMSD calculation purposes (bold residues correspond to nonconserved residues among human and murine iNOS). These residues were chosen because delimiting the access route to the active site during the SMD trajectories.

For each ligand, only the five best predicted poses (five best scores) were conserved, and their RMSD against the targeted, X-ray position were computed within Pymol. We hypothesized that the positions in human iNOSOxy might be the same as in murine iNOSOxy as the overall sequence conservation between the two enzymes is very high (>95% identity). The minimum RMSD values observed for each ligand as compared to the crystallographic position were reported in Figure 7 and showed that the docking in the set of 20 representative conformations (graphs on the bottom) significantly improved the results for many ligands with decreased RMSD values; some representative cases are reported for the 1M8H, 3E6O, 1M8D, and 3E7I ligands in Figure 8. These ligands were not correctly located in the 1NSI

structure (boxes on the top), whereas they were much better placed in the set of 20 representative structures of the enzyme (boxes in the bottom). This was essentially due to motions of both Arg266 and Arg388 and also of Gln263. For other ligands including 1DD7, 2ORO, 2ORP, 2ORQ, 2ORR and 2ORT, the set of generated structures failed to improve the docking results. This was essentially because these ligands constitute inhibitors of dimerization and bind to the monomeric form of iNOS. It is difficult to predict their correct orientation as most of these molecules completely bend inside the active site. This shows that rotation of the Glu377 is not sufficient to predict their correct orientation from calculations. For these ligands, this is much more a limitation of the docking method than a non appropriateness of the data.

As expected, this observation confirmed that docking into iNOSOxy required taking care of the flexibility of the substrate access channel to the active site. It also demonstrated that molecular dynamics simulations might be useful to refine docking predictions in NOSs, particularly in the human iNOS isoforms.

■ DISCUSSION/CONCLUSION

In this study, we explored the possible unbinding/binding route of L-Arg out from/toward the human iNOS active site. As the structure of a full NOS enzyme has not yet been solved, this study was performed considering only the dimer of iNOSOxy excluding reductase and calmodulin domains. Nevertheless, it could be noticed that a close match between spectroscopic properties, binding affinities (K_d), and IC_{50} values between iNOSOxy and the full-length iNOS has been reported.^{1,2,4,6} Therefore, the presented results might apply to the full-length iNOS.

Another crucial question might deal with the driving force, e.g., what is (are) the phenomena that promote(s), without applying any constraint (as in the present study), the entry of the ligand in the mouth of the channel and then drive(s) it toward its final position in the active site? The electrostatic field lines, as

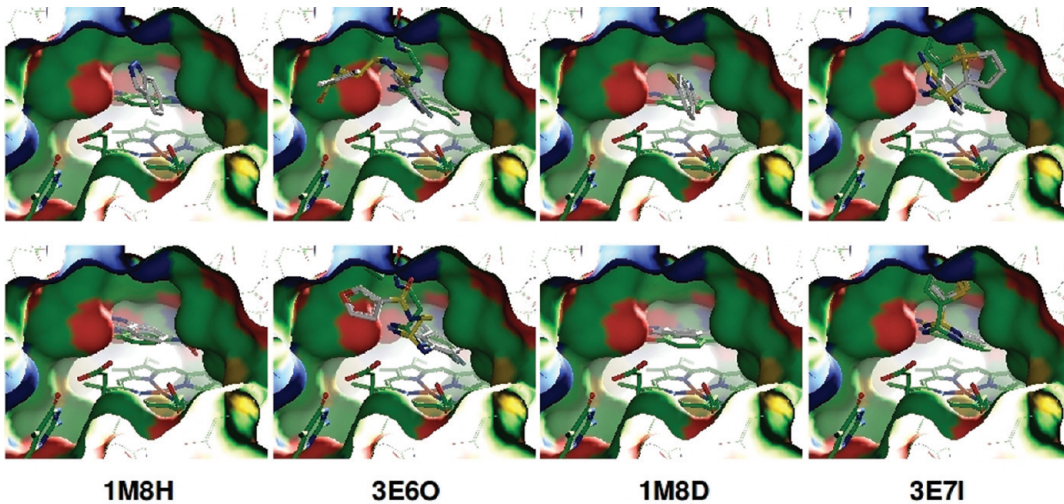


Figure 8. Docking results of some of the iNOS ligands that display an improved positioning as deduced from Figure 7. In each box, the known crystallographic position was reported in green, and the best position (min RMSD) was reported in white for either the starting human iNOS structure (upper) or the set of 20 representative conformations of the target (bottom). The limitation on the upper line was essentially due to bad contacts that were successfully removed on the bottom.

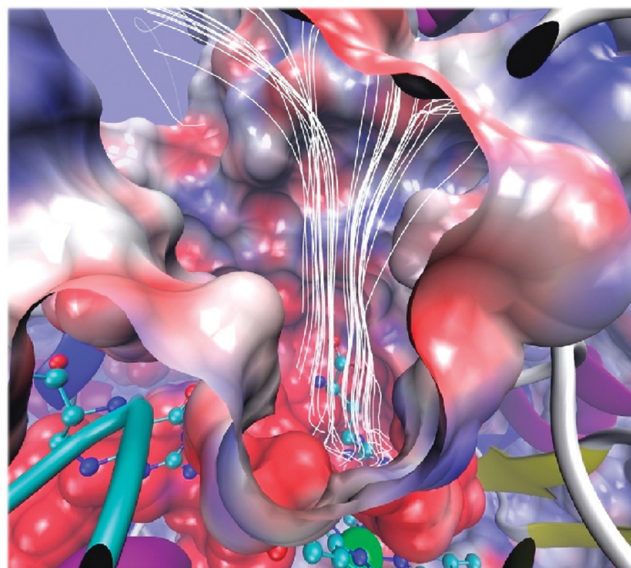


Figure 9. Electrostatic field lines in the access channel that may drive the binding of L-Arg on longer time-scales.

computed with VMD from the crystallographic structure of human iNOS, are represented in Figure 9 and show that electrostatic gradients might drive the ligand toward its final position. This driving force might occur on longer time scale than those described in the present paper and involves much larger amplitude motions as described above with possible anticooperative movements between monomers.

Our results nicely agree with available data on L-Arg binding to iNOS. Nevertheless, other structural rearrangements that are also involved in this binding were neglected because of the incapacity of molecular dynamics simulations to reproduce them; these included loop inversion around the BH4 cofactor and large conformational transitions around the cysteines/zinc complex at the dimer interface.

Due to the high degree of sequence and structure conservation in the active site among the three NOSs isoforms, the design of

inhibitors with high specificity for the inducible NOS is a difficult task. As a consequence, data describing the dynamic of binding in the access channel to the active site may reveal useful for further studies. In that context, we showed that the generated models are already useful for the refinement of docking experiments, and a more exhaustive study is under progress. In this study we were concerned with L-Arg binding to the inducible isoform of NOS. Perspectives to this work include related studies performed on human nNOS and eNOS and on other classes of ligands to test the efficiency of such a protocol to discriminate between ligands with different affinities or specificities for one isoform. Nevertheless, extension of our findings to eNOS and nNOS will require caution, especially due to local structural rearrangements that can occur at the N-terminal ends of these two constitutive NOS isoforms.

■ ASSOCIATED CONTENT

S Supporting Information. Figure S1: Root mean square fluctuations (RMSF) of the C α of the protein computed along the entire initial trajectory. On the backbone representation, the more flexible regions are reported in red, whereas rigid regions are reported in blue. On the graph, the black curve stands for the computed theoretical B-factors (RMSF), whereas the red curve corresponds to the experimental values stored in the PDB: 1NSI file. The dashed black line corresponds to the mean RMSF computed for the protein. This material is available free of charge via the Internet at <http://pubs.acs.org>.

■ AUTHOR INFORMATION

Corresponding Author

*E-mail: nicolas.floquet@univ-montp1.fr.

■ ACKNOWLEDGMENT

We thank Dr. Anne-Dominique Lajoix (CNRS UMR 5232, Montpellier) for valuable discussions. We also thank Remy Dernat and Bruno Maurel (IBMM, CNRS UMR 5247) for technical assistance.

■ REFERENCES

- (1) Pfeiffer, S.; Mayer, B.; Hemmens, B. Nitric oxide: Chemical puzzles posed by a biological messenger. *Angew. Chem., Int. Ed.* **1999**, *38*, 1715–1731.
- (2) Alderton, W. K.; Cooper, C. E.; Knowles, R. G. Nitric oxide synthases: structure, function and inhibition. *Biochem. J.* **2001**, *357*, 593–615.
- (3) Geller, D. A.; Billiar, T. R. Molecular biology of nitric oxide synthases. *Cancer Metastasis Rev.* **1998**, *17*, 7–23.
- (4) Gosh, D. K.; Salerno, J. C. Nitric oxide synthases: Domain structure and alignment in enzyme function and control. *Front. Biosci.* **2003**, *8*, 193–209.
- (5) Masters, B. S.; McMillan, K.; Sheta, E. A.; Nishimura, J. S.; Roman, L. J.; Martasek, P. Neuronal nitric oxide synthase, a modular enzymes formed by convergent evolution: Structure studies of a cysteine thiolate-ligated heme protein that hydroxylates L-arginine to produce NO as a cellular signal. *FASEB J.* **1996**, *10*, 552–558.
- (6) Stuehr, D. J. Mammalian nitric oxide synthases. *Biochim. Biophys. Acta* **1999**, *1411*, 217–230.
- (7) Perreault, M.; Marette, A. Targeted disruption of inducible nitric oxide synthase protects against obesity-linked insulin resistance in muscle. *Nat. Med.* **2001**, *7*, 1138–1143.
- (8) Hilliquin, P.; Borderie, D.; Hernvann, A.; Menkes, C. J.; Ekindjian, O. G. Nitric oxide as S-nitrosoproteins in rheumatoid arthritis. *Arthritis Rheum.* **1997**, *40*, 1512–1517.
- (9) Brown, G. C.; Bal-Price, A. Inflammatory neurodegeneration mediated by nitric oxide, glutamate, and mitochondria. *Mol. Neurobiol.* **2003**, *27*, 325–355.
- (10) Floyd, R. A. Antioxidants, oxidative stress, and degenerative neurological disorders. *Proc. Soc. Exp. Biol. Med.* **1999**, *222*, 236–245.
- (11) Piehl, F.; Lidman, O. Neuroinflammation in the rat-CNS cells and their role in the regulation of immune reactions. *Immunol. Rev.* **2001**, *184*, 212–225.
- (12) Carvalho-Filho, M. A.; Ueno, M.; Hirabara, S. M.; Seabra, A. B.; Carvalheira, J. B.; de Oliveira, M. G.; Velloso, L. A.; Curi, R.; Saad, M. J. S-nitrosation of the insulin receptor, insulin receptor substrate 1, and protein kinase B/Akt: a novel mechanism of insulin resistance. *Diabetes* **2005**, *54*, 959–967.
- (13) Noronha, B. T.; Li, J. M.; Wheatcroft, S. B.; Shah, A. M.; Kearney, M. T. Inducible nitric oxide synthase has divergent effects on vascular and metabolic function in obesity. *Diabetes* **2005**, *54*, 1082–1089.
- (14) Ekmekcioglu, S.; Ellerhorst, J. A.; Prieto, V. G.; Johnson, M. M.; Broemeling, L. D.; Grimm, E. A. Tumor iNOS predicts poor survival for stage III melanoma patients. *Int. J. Cancer* **2006**, *119*, 861–866.
- (15) Ekmekcioglu, S.; Tang, C. H.; Grimm, E. A. NO news is not necessarily good news in cancer. *Curr. Cancer Drug Targets* **2005**, *5*, 103–115.
- (16) Rimoldi, J. M.; Chimote, S. S. Inhibition of inducible nitric oxide synthase. *Curr. Opin. Drug Discovery Dev.* **1998**, *1*, 183–191.
- (17) Crane, B. R.; Arvai, A. S.; Ghosh, D. K.; Wu, C.; Getzoff, E. D.; Stuehr, D. J.; Tainer, J. A. Structure of nitric oxide oxygenase dimer with pterin and substrate. *Science* **1998**, *279*, 2121–2126.
- (18) Fischmann, T. O.; Hruza, A.; Niu, X. D.; Fossetta, J. D.; Lunn, C. A.; Dolphin, E.; Prongay, A. J.; Reichert, P.; Lundell, D. J.; Narula, S. K.; Weber, P. C. Structural characterization of nitric oxide synthase isoforms reveals striking active-site conservation. *Nat. Struct. Biol.* **1999**, *6*, 233–242.
- (19) Li, H.; Raman, C. S.; Glaser, C. B.; Blasko, E.; Young, T. A.; Parkinson, J. F.; Whitlow, M.; Poulos, T. L. Crystal structures of zinc-free and -bound heme domain of human inducible nitric-oxide synthase. Implications for dimer stability and comparison with endothelial nitric-oxide synthase. *J. Biol. Chem.* **1999**, *274*, 21276–21284.
- (20) Raman, C. S.; Li, H.; Martasek, P.; Kral, V.; Masters, B. S.; Poulos, T. L. Crystal structure of constitutive endothelial nitric oxide synthase: A paradigm for pterin function involving a novel metal center. *Cell* **1998**, *95*, 939–950.
- (21) Li, H.; Igarashi, J.; Jamal, J.; Yang, W.; Poulos, T. L. Structural studies of constitutive nitric oxide synthases with diatomic ligands bound. *J. Biol. Inorg. Chem.* **2006**, *11*, 753–768.
- (22) Li, H.; Poulos, T. L. Structure-function studies on nitric oxide synthases. *J. Inorg. Biochem.* **2005**, *99*, 293–305.
- (23) Ji, H.; Li, H.; Flinspach, M.; Poulos, T. L.; Silverman, R. B. Computer modeling of selective regions in the active site of nitric oxide synthases: implication for the design of isoform-selective inhibitors. *J. Med. Chem.* **2003**, *46*, 5700–5711.
- (24) Silverman, R. B. Design of selective neuronal nitric oxide synthase inhibitors for the prevention and treatment of neurodegenerative diseases. *Acc. Chem. Res.* **2009**, *42*, 439–451.
- (25) Garcin, E. D.; Arvai, A. S.; Rosenfeld, R. J.; Kroeger, M. D.; Crane, B. R.; Andersson, G.; Andrews, G.; Hamley, P. J.; Mallinder, P. R.; Nicholls, D. J.; St-Gallay, S. A.; Tinker, A. C.; Gensmantel, N. P.; Mete, A.; Cheshire, D. R.; Connolly, S.; Stuehr, D. J.; Aberg, A.; Wallace, A. V.; Tainer, J. A.; Getzoff, E. D. Anchored plasticity opens doors for selective inhibitor design in nitric oxide synthase. *Nat. Chem. Biol.* **2008**, *4*, 700–707.
- (26) Isralewitz, B.; Baudry, J.; Gullingsrud, J.; Kosztin, D.; Schulten, K. Steered molecular dynamics investigations of protein function. *J. Mol. Graphics Modell.* **2001**, *19*, 13–25.
- (27) Mehboob, S.; Guo, L.; Fu, W.; Mittal, A.; Yau, T.; Truong, K.; Johlfs, M.; Long, F.; Fung, L. W.; Johnson, M. E. Glutamate racemase dimerization inhibits dynamic conformational flexibility and reduces catalytic rates. *Biochemistry* **2009**, *48*, 7045–7055.
- (28) Vashisth, H.; Abrams, C. F. Ligand escape pathways and (un)binding free energy calculations for the hexameric insulin-phenol complex. *Biophys. J.* **2008**, *95*, 4193–4204.
- (29) Shen, J.; Li, W.; Liu, G.; Tang, Y.; Jiang, H. Computational insights into the mechanism of ligand unbinding and selectivity of estrogen receptors. *J. Phys. Chem. B* **2009**, *113*, 10436–10444.
- (30) Wang, J.; Wang, W.; Kollman, P. A.; Case, D. A. Automatic atom type and bond type perception in molecular mechanical calculations. *J. Mol. Graphics Modell.* **2006**, *25*, 247–260.
- (31) Wang, J.; Wolf, R. M.; Caldwell, J. W.; Kollman, P. A.; Case, D. A. Development and testing of a general amber force field. *J. Comput. Chem.* **2004**, *25*, 1157–1174.
- (32) Brooks, B. R.; Brooks, C. L.; Mackerell, A. D., Jr.; Nilsson, L.; Petrella, R. J.; Roux, B.; Won, Y.; Archontis, G.; Bartels, C.; Boresch, S.; Caflisch, A.; Caves, L.; Cui, Q.; Dinner, A. R.; Feig, M.; Fischer, S.; Gao, J.; Hodoscek, M.; Im, W.; Kuczera, K.; Lazaridis, T.; Ma, J.; Ovchinnikov, V.; Paci, E.; Pastor, R. W.; Post, C. B.; Pu, J. Z.; Schaefer, M.; Tidor, B.; Venable, R. M.; Woodcock, H. L.; Wu, X.; Yang, W.; York, D. M.; Karplus, M. CHARMM: the biomolecular simulation program. *J. Comput. Chem.* **2009**, *30*, 1545–1614.
- (33) Foloppe, N.; Nilsson, L. The glutaredoxin -C-P-Y-C- motif: influence of peripheral residues. *Structure* **2004**, *12*, 289–300.
- (34) Foloppe, N.; Sagemark, J.; Nordstrand, K.; Berndt, K. D.; Nilsson, L. Structure, dynamics and electrostatics of the active site of glutaredoxin 3 from Escherichia coli: comparison with functionally related proteins. *J. Mol. Biol.* **2001**, *310*, 449–470.
- (35) Phillips, J. C.; Braun, R.; Wang, W.; Gumbart, J.; Tajkhorshid, E.; Villa, E.; Chipot, C.; Skeel, R. D.; Kale, L.; Schulten, K. Scalable molecular dynamics with NAMD. *J. Comput. Chem.* **2005**, *26*, 1781–1802.
- (36) Trott, O.; Olson, A. J. AutoDock Vina: improving the speed and accuracy of docking with a new scoring function, efficient optimization, and multithreading. *J. Comput. Chem.* **2010**, *31*, 455–461.
- (37) Morris, G. M.; Huey, R.; Lindstrom, W.; Sanner, M. F.; Belew, R. K.; Goodsell, D. S.; Olson, A. J. AutoDock4 and AutoDockTools4: Automated docking with selective receptor flexibility. *J. Comput. Chem.* **2009**, *30*, 2785–2791.
- (38) Morris, G. M.; Huey, R.; Lindstrom, W.; Sanner, M. F.; Belew, R. K.; Goodsell, D. S.; Olson, A. J. AutoDock4 and AutoDockTools4: Automated docking with selective receptor flexibility. *J. Comput. Chem.* **2009**, *30*, 2785–2791.
- (39) Floquet, N.; Hery-Huynh, S.; Dauchez, M.; Derreumaux, P.; Tamburro, A. M.; Alix, A. J. Structural characterization of VGVAPG, an elastin-derived peptide. *Biopolymers* **2004**, *76*, 266–280.

- (40) McMillan, K.; Adler, M.; Auld, D. S.; Baldwin, J. J.; Blasko, E.; Browne, L. J.; Chelsky, D.; Davey, D.; Dolle, R. E.; Eagen, K. A.; Erickson, S.; Feldman, R. I.; Glaser, C. B.; Mallari, C.; Morrissey, M. M.; Ohlmeyer, M. H.; Pan, G.; Parkinson, J. F.; Phillips, G. B.; Polokoff, M. A.; Sigal, N. H.; Vergona, R.; Whitlow, M.; Young, T. A.; Devlin, J. J. Allosteric inhibitors of inducible nitric oxide synthase dimerization discovered via combinatorial chemistry. *Proc. Natl. Acad. Sci. U.S.A.* **2000**, *97*, 1506–1511.
- (41) Chen, P. F.; Berka, V.; Wu, K. K. Differential effects of mutations in human endothelial nitric oxide synthase at residues Tyr-357 and Arg-365 on L-arginine hydroxylation and ⁶N-hydroxy-L-arginine oxidation. *Arch. Biochem. Biophys.* **2003**, *411*, 83–92.
- (42) Sato, Y.; Sagami, I.; Matsui, T.; Shimizu, T. Unusual role of Tyr588 of neuronal nitric oxide synthase in controlling substrate specificity and electron transfer. *Biochem. Biophys. Res. Commun.* **2001**, *281*, 621–626.
- (43) Wang, Z. Q.; Wei, C. C.; Sharma, M.; Pant, K.; Crane, B. R.; Stuehr, D. J. A conserved Val to Ile switch near the heme pocket of animal and bacterial nitric-oxide synthases helps determine their distinct catalytic profiles. *J. Biol. Chem.* **2004**, *279*, 19018–19025.
- (44) Raman, C. S.; Li, H.; Martasek, P.; Southan, G.; Masters, B. S.; Poulos, T. L. Crystal structure of nitric oxide synthase bound to nitro indazole reveals a novel inactivation mechanism. *Biochemistry* **2001**, *40*, 13448–13455.
- (45) Rosenfeld, R. J.; Garcin, E. D.; Panda, K.; Andersson, G.; Aberg, A.; Wallace, A. V.; Morris, G. M.; Olson, A. J.; Stuehr, D. J.; Tainer, J. A.; Getzoff, E. D. Conformational changes in nitric oxide synthases induced by chloroxazone and nitroindazoles: crystallographic and computational analyses of inhibitor potency. *Biochemistry* **2002**, *41*, 13915–13925.
- (46) Davey, D. D.; Adler, M.; Arnaiz, D.; Eagen, K.; Erickson, S.; Guilford, W.; Kenrick, M.; Morrissey, M. M.; Ohlmeyer, M.; Pan, G.; Paradkar, V. M.; Parkinson, J.; Polokoff, M.; Saionz, K.; Santos, C.; Subramanyam, B.; Vergona, R.; Wei, R. G.; Whitlow, M.; Ye, B.; Zhao, Z. S.; Devlin, J. J.; Phillips, G. Design, synthesis, and activity of 2-imidazol-1-ylpyrimidine derived inducible nitric oxide synthase dimerization inhibitors. *J. Med. Chem.* **2007**, *50*, 1146–1157.
- (47) Crane, B. R.; Arvai, A. S.; Gachhui, R.; Wu, C.; Ghosh, D. K.; Getzoff, E. D.; Stuehr, D. J.; Tainer, J. A. The structure of nitric oxide synthase oxygenase domain and inhibitor complexes. *Science* **1997**, *278*, 425–431.
- (48) Matter, H.; Kumar, H. S.; Fedorov, R.; Frey, A.; Kotsonis, P.; Hartmann, E.; Frohlich, L. G.; Reif, A.; Pfleiderer, W.; Scheurer, P.; Ghosh, D. K.; Schlichting, I.; Schmidt, H. H. Structural analysis of isoform-specific inhibitors targeting the tetrahydrobiopterin binding site of human nitric oxide synthases. *J. Med. Chem.* **2005**, *48*, 4783–4792.
- (49) Bahar, I.; Lezon, T. R.; Bakan, A.; Shrivastava, I. H. Normal Mode Analysis of Biomolecular Structures: Functional Mechanisms of Membrane Proteins. *Chem. Rev.* **2010**, *110*, 1463–1497.
- (50) Bakan, A.; Bahar, I. The intrinsic dynamics of enzymes plays a dominant role in determining the structural changes induced upon inhibitor binding. *Proc. Natl. Acad. Sci. U.S.A.* **2009**, *106*, 14349–14354.
- (51) Floquet, N.; Marechal, J. D.; Badet-Denisot, M. A.; Robert, C. H.; Dauchez, M.; Perahia, D. Normal mode analysis as a prerequisite for drug design: application to matrix metalloproteinases inhibitors. *FEBS Lett.* **2006**, *580*, 5130–5136.
- (52) Gorren, A. C.; List, B. M.; Schrammel, A.; Pitters, E.; Hemmens, B.; Werner, E. R.; Schmidt, K.; Mayer, B. Tetrahydrobiopterin-free neuronal nitric oxide synthase: evidence for two identical highly anticooperative pteridine binding sites. *Biochemistry* **1996**, *35*, 16735–16745.
- (53) Gorren, A. C.; Schrammel, A.; Schmidt, K.; Mayer, B. Thiols and neuronal nitric oxide synthase: complex formation, competitive inhibition, and enzyme stabilization. *Biochemistry* **1997**, *36*, 4360–4366.
- (54) Humphrey, W.; Dalke, A.; Schulter, K. VMD: visual molecular dynamics. *J. Mol. Graphics* **1996**, *14* (27–28), 33–38.